



**HAL**  
open science

## Cellulose NanoCrystals-Fibrin Nanocomposite Hydrogels Promoting Myotube Formation

Kun Wang, Gervaise Mosser, Bernard Haye, Niki Baccile, Patrick Le Griel,  
Petra Pernot, Bernard Cathala, Léa Trichet, Thibaud Coradin

► **To cite this version:**

Kun Wang, Gervaise Mosser, Bernard Haye, Niki Baccile, Patrick Le Griel, et al.. Cellulose NanoCrystals-Fibrin Nanocomposite Hydrogels Promoting Myotube Formation. *Biomacromolecules*, 2021, 22 (6), pp.2740-2753. 10.1021/acs.biomac.1c00422 . hal-03227208

**HAL Id: hal-03227208**

**<https://hal.science/hal-03227208v1>**

Submitted on 17 May 2021

**HAL** is a multi-disciplinary open access archive for the deposit and dissemination of scientific research documents, whether they are published or not. The documents may come from teaching and research institutions in France or abroad, or from public or private research centers.

L'archive ouverte pluridisciplinaire **HAL**, est destinée au dépôt et à la diffusion de documents scientifiques de niveau recherche, publiés ou non, émanant des établissements d'enseignement et de recherche français ou étrangers, des laboratoires publics ou privés.

# Cellulose NanoCrystals-Fibrin Nanocomposite Hydrogels Promoting Myotube Formation

*Kun Wang,<sup>†</sup> Gervaise Mosser,<sup>†</sup> Bernard Haye,<sup>†</sup> Niki Baccile,<sup>†</sup> Patrick Le Griel,<sup>†</sup> Petra Pernot,<sup>§</sup>  
Bernard Cathala,<sup>‡</sup> Léa Trichet,<sup>†</sup> Thibaud Coradin<sup>†,\*</sup>*

<sup>†</sup> Sorbonne Université, CNRS, Laboratoire de Chimie de la Matière Condensée de Paris, 75005  
Paris, France.

<sup>§</sup> ESRF – The European Synchrotron, CS40220, 38043 Grenoble, France

<sup>‡</sup> INRAE, UR BIA, 44316 Nantes, France.

ABSTRACT. Cellulose Nanocrystals have been widely studied as fillers to form reinforced nanocomposites with a wide range of applications, including the biomedical area. Here, we evaluated the possibility to combine them with fibrinogen and obtain fibrin hydrogels with improved mechanical stability as potential cellular scaffolds. In diluted conditions at neutral pH, it was evidenced that fibrinogen could adsorb on cellulose nanocrystals in a two-step process, favoring their alignment under flow. Composite hydrogels could be prepared from concentrated fibrinogen solutions and nanocrystals amounts up to 0.3 w%. Cellulose nanocrystals induced a significant modification of initial fibrin fibrillogenesis and final fibrin network structure, and storage moduli of all nanocomposites were larger than that of pure fibrin hydrogels. Moreover, optimal conditions were found that promoted muscle cells differentiation and formation of long myotubes. These results provide original insights on the interactions of cellulose nanocrystals with proteins with key physiological functions and offer new perspectives for the design of injectable fibrin-based formulations.

**Keywords:** fibrin, cellulose nanocrystals, hydrogels, nanocomposites, myotubes

## Introduction

After vessel injury, a key phase of the blood clotting process is the interaction between thrombin and fibrinogen to form the fibrin clot.<sup>1</sup> Thrombin cleaves fibrinopeptides from the central domain of the fibrinogen chain, leading to the formation of fibrin molecules that self-assemble to form fibrils, leading to clot formation.<sup>1-3</sup> *In vivo*, under the effect of Factor XIII, cross-linking significantly contributes to increase fiber thickness and clot stiffness.<sup>4,5</sup> However, fibrin gels resulting from fibrinogen and thrombin mixtures without Factor XIII *in vitro* show moderate mechanical properties and fast biodegradability, which limit their range of applications as biomaterials.<sup>6,7</sup>

To address this point, an increasing amount of studies focus on fibrin-based mixed or composite hydrogels incorporating other biopolymers, such as chitosan,<sup>8,9</sup> gelatin,<sup>10,11</sup> collagen,<sup>12-15</sup> alginate,<sup>16,17</sup> or (oxidized) cellulose,<sup>18-20</sup> that are used in wound healing, drug delivery, bone regeneration and tissue engineering. Among these, oxidized cellulose is of particular interest because it is, like fibrin, a hemostatic agent that can accelerate blood coagulation by immediately extracting fluid from the blood and entrapping blood proteins, platelets, red blood cells, and other active ingredients.<sup>21</sup>

Among the various forms of commercially-available cellulose-derived products, cellulose nanocrystals (CNC) have been widely studied for an impressive range of applications.<sup>22-29</sup> CNCs are mainly produced by acid hydrolysis of cellulose, while controlled oxidation, enzymatic and ionic liquids treatment also can help the formation of CNC.<sup>25,30</sup> Different cellulose sources and hydrolysis conditions endow various dimensions to CNCs. For example, plant-sourced CNCs

present diameters of 5-30 nm and length of 100–500 nm.<sup>30</sup> CNC-based composites are promising candidates for biomedical applications because of their outstanding mechanical stability, controllable morphology, as well as high biocompatibility and biodegradability.<sup>22,27</sup> Several composites associating CNCs with proteins, including collagen and gelatin, have been described, highlighting the ability of these proteins to improve the mechanical properties of the CNC gels.<sup>31-</sup>  
<sup>34</sup> However, to our knowledge, only one study was previously dedicated to the combination of CNCs with fibrin, for the design small-diameter replacement vascular graft.<sup>35</sup> However, CNCs were oxidized to enhance their interaction with fibrin and, as in many examples of CNC-polymer nanocomposites,<sup>36-38</sup> these materials were prepared as casted films and no example of similar bulk hydrogels using pristine CNCs was reported so far.

In this context, the present aimed at designing nanocomposite biomaterials where CNCs could act both as fillers to reinforce fibrin hydrogels and as nanoscale substrates to tune cell behavior.<sup>39,40</sup> Interactions of fibrinogen with CNCs were first studied in diluted conditions with the aim of evidencing protein adsorption and its impact on both fibrinogen conformation and CNC organization. In a second step, nanocomposite hydrogels were prepared and characterized both from a structural and mechanical perspective. Finally, the fate of mouse myoblasts seeded on these nanocomposite hydrogels was studied to evaluate their potential for skeletal muscle repair.<sup>41</sup>

## Experimental Section

**Materials.** Fibrinogen (Fbg) from bovine plasma (~340 kDa, > 90 % clottable protein, EMD Millipore) and thrombin from bovine plasma (~38 kDa, 40-60 % protein, 40-300 NIH units/mg, Sigma) were used. Cellulose NanoCrystals (CNC) were obtained from Celluforce as a spray dried powder in the sodium salt form. CNCs were produced by sulfuric acid hydrolysis of

bleached kraft pulp. According to Cellulforce specifications, the CNCs have a particle cross-section of 2.3-4.5 nm, particle length of 44-108 nm, crystalline fraction of 0.88 (by X-ray diffraction) and sulfate content of 246-261 mmol.kg<sup>-1</sup>. Except when noted, all suspensions were prepared in a 20 mM citrate buffer (sodium citrate-HCl, pH 7.2)

**Dynamic Light Scattering.** The apparent hydrodynamic diameter of CNC, Fbg and CNC mixed with increasing amounts of fibrinogen was measured by Dynamic Light Scattering (Zetasizer Nano ZSE, MALVERN) at 37 °C. A 1 mL suspension of CNC (0.025 mg.mL<sup>-1</sup>) was studied first, and then 20 µL of fibrinogen (0.05 mg.mL<sup>-1</sup>) was added and left to react for 10 min before the next measurements. The operation was repeated to obtain Fbg:CNC weight ratio between 0:1 and 2:1

**Zeta Potential Measurements.** The zeta potential ( $\zeta$ ) of pure CNC, Fbg and CNC mixed with increasing amounts of fibrinogen were measured using a Zetasizer Nano ZSE (MALVERN) at 37 °C. A 1 mL suspension of CNC (0.25 mg.mL<sup>-1</sup>) was studied first, and then 50 µL of fibrinogen (0.50 mg.mL<sup>-1</sup>) was added and left to react for 10 min before the next measurements. The operation was repeated to obtain Fbg:CNC weight ratio between 0:1 and 2:1.

**Protein Sorption Experiments.** Standard curves for protein quantitation assays were first measured using fibrinogen solutions in citrate buffer in the 0-0.50 mg.mL<sup>-1</sup> concentration range following the protocol of the bicinchoninic acid (BCA) protein Assay kit (Thermo Scientific™ Pierce™). For sorption experiments, samples were prepared by mixing 1 mL of the CNC suspension (0.25 mg.mL<sup>-1</sup>) with different volumes of fibrinogen (0.50 mg.mL<sup>-1</sup>) to obtain Fbg:CNC weight ratio between 0:1 and 2:1, was mixed for 10 min. The suspension was then centrifuged for 1 h at 23,000 rpm and the supernatant titrated for fibrinogen. The same mixture

without centrifugation was used as control. Sorption isotherm was established based on concentration of fibrinogen remaining in solution after adsorption allowing to calculate the amount of fibrinogen adsorbed on CNCs.

**Circular Dichroism Measurements.** The conformation of fibrinogen as such or in the presence of increasing amounts of CNC was studied by Circular Dichroism (CD) measurements in the 185-300 nm range in Quartz cuvettes with an optical pass length of 0.1 mm on a JASCO J810 spectropolarimeter. Samples were prepared by mixing 1 mL of the fibrinogen solution (0.5 mg.mL<sup>-1</sup>) with 0 to 900  $\mu$ L of CNC (1.0 mg.mL<sup>-1</sup>) to obtain Fbg:CNC weight ratio between 1:0 and 2.5:1. CD measurements of Fbg solutions mixed with similar volumes of citrate buffer were performed as controls to evaluate the effect of dilution on Fbg spectrum.

**Small Angle X-ray Scattering.** SAXS experiments were performed on the BioSAXS BM29 beamline at the ESRF synchrotron facility (Experiment: MX2311, Grenoble, France) using 12.5 keV energy and a sample-to-detector distance of 2.867 m, imposed by the beamline standard configuration. The energy is calibrated by measuring the L<sub>I</sub> and L<sub>III</sub> edges of platinum and the sample-to-detector distance is determined using silver behenate ( $d_{\text{ref}} = 58.38 \text{ \AA}$ ).<sup>42,43</sup> For this experiment, we employ the automatic sample changer for liquids using the 96-well plates and about 100  $\mu$ L of each sample.<sup>44</sup> The liquid sample is automatically loaded into a 1 mm quartz glass capillary and ten acquisitions of 1 s each are taken as the sample passes the beam. Individual frames are systematically controlled for systematic changes and averaged for better statistics. Eventual changes can be either due to intrinsic sample heterogeneity or radiation damage. The signal of the Pilatus 2M 2D detector, used to record the data, is integrated azimuthally with PyFAI to obtain the scattered intensity  $I(q)$  vs.  $q$  spectrum ( $q = 4\pi \sin \theta / \lambda$ , where  $2\theta$  is the scattering

angle) after masking systematically wrong pixels and the beam stop shadow.<sup>45</sup> Absolute intensity units were determined by measuring the scattering signal of water ( $0.01632 \text{ cm}^{-1}$  at  $20^\circ\text{C}$ ). Fibrinogen solutions ( $2\text{-}20 \text{ mg.mL}^{-1}$ ) were first studied and then mixed with  $5 \text{ mg.mL}^{-1}$  CNC suspensions to obtain CNC:Fbg 1:0 to 1:1 ratio for further analysis. Experiments were performed at  $25^\circ\text{C}$  immediately after sample preparation.

**Steady Shear Rheology.** A 1 mL CNC suspension ( $0.5 \text{ mg.mL}^{-1}$ ) was mixed with 1 mL of citrate buffer or fibrinogen solutions at different concentrations ( $1 \text{ mg.mL}^{-1}$ ,  $0.5 \text{ mg.mL}^{-1}$  and  $0.25 \text{ mg.mL}^{-1}$ ). Reference samples were obtained mixing 1 mL of citrate buffer with 1 mL of the same fibrinogen solutions. The apparent viscosity was measured at increasing shear rate by steady shear experiments in a cone-plate geometry (CP25-1) using a MCR 302 rheometer from Anton Paar

**Cryo-Transmission Electron Microscopy.** Cryo-TEM examination of CNC ( $0.25 \text{ mg.mL}^{-1}$ ), Fbg ( $0.50 \text{ mg.mL}^{-1}$ ) and mixtures at Fbg:CNC weight ratio of 1:2, 1:1 and 2:1 were carried out on an FEI Tecnai 120 twin microscope operated at 120 kV and equipped with a Gatan Orius CCD numeric camera. The sample holder is a Gatan Cryoholder instrument (Gatan 626DH, Gatan). Digital Micrograph software was used for image acquisition. Cryofixation was performed using a homemade cryofixation device. Suspensions were deposited on a glow-discharged holey carbon-coated TEM nickel grid (Quantifoil R2/2). Excess suspension was removed, and the grid was immediately plunged into nitrogen-cooled liquid ethane before being transferred into liquid nitrogen. All grids were kept at liquid nitrogen temperature throughout whole experimentation. Cryo-TEM images were treated and analyzed using Fiji software, available free of charge at the developer's web site.



**Formation of Fibrin-CNC hydrogels.** To prepare nanocomposite hydrogels, 100  $\mu\text{L}$  of citrate buffer or CNC suspensions (5-30  $\text{mg}\cdot\text{mL}^{-1}$ ) was mixed with 900  $\mu\text{L}$  of fibrinogen solution (20  $\text{mg}\cdot\text{mL}^{-1}$  or 30  $\text{mg}\cdot\text{mL}^{-1}$ ) dispensed in 12 well-plates and then 2  $\mu\text{L}$  or 8  $\mu\text{L}$ , respectively, of thrombin (200  $\text{U}\cdot\text{mL}^{-1}$ ) was added.

**UV-visible Spectrophotometry.** Fibrillogenesis was followed by UV-visible absorption measurements at  $\lambda = 400$  nm at room temperature. For this purpose, the above-described fibrinogen or fibrinogen-CNC suspensions were first mixed in a 1.5 mL cuvette and the absorbance was measured. After 30 s, the suspension was transferred to an Eppendorf tube, the above-mentioned thrombin solution was added and the mixture was transferred back to cuvette, with a fixed duration of the whole process of 30 s. The time evolution of absorbance was then recorded for the next 29 minutes, at a rate of 15 measurements per minute.

**Rheological Studies of Hydrogels.** The evolution of the rheological properties of the gels prepared in the same conditions was measured using a MCR 302 rheometer from Anton Paar. Fibrinogen or fibrinogen-CNC suspensions with added thrombin were placed on the sample holder fitted with cone and plate geometry with a fixed gap width. Measurements were performed at 37°C at constant amplitude and angular frequency ( $\gamma = 0.1\%$ ,  $\omega = 0.5$   $\text{rad}\cdot\text{s}^{-1}$ ).

**Transmission Electron Microscopy.** Before observation, fibrin and fibrin-CNC hydrogels were sequentially fixed with paraformaldehyde, glutaraldehyde and osmium tetroxide 4 wt% and then subsequently dehydrated using ethanol baths, progressively impregnated with propylene oxide and incorporated in araldite resin prior to sectioning (Leica microtome). Sections were imaged by TEM on a Tecnai Spirit G2 operating at 120 kV (FEI Company, Philips, Netherlands). Images were recorded on a Gatan CCD Oriuscamera.

**Cell Culture and Seeding on Hydrogels.** C2C12 cells were grown in DMEM medium (high glucose, from Merck) supplemented with 10% fetal bovine serum (from Gibco) and 1% penicillin/streptomycin at 37°C in a humidified incubator with 5% CO<sub>2</sub>, and passaged every 2 days. 1mL of cell suspension at passage 14 containing 40,000 C2C12 cells were seeded on the pure fibrin and composite hydrogels prepared in 12-well plates. After 4, 6, 8 and 10 days, the medium was discarded and the Alamar Blue reagent (800 μL of a 0.1 mg.mL<sup>-1</sup> solution, from ThermoFisher) was added to the wells. After 4 h incubation at 37 °C, absorbance values at 570 nm and 600 nm were measured to obtain the reduction percentage of Alamar Blue.

**Fluorescence Microscopy.** The ability of seeded cells to differentiate and form myotubes was also studied. After the formation of gels, 1 mL of growth medium supplemented with 6-Aminocaproic acid (ACA, from Sigma-Aldrich) (2mg.mL<sup>-1</sup>) was added on the top of the gels and renewed after 2 days. After 4 days, the previous growth medium was replaced by 1 mL of differentiation medium (DMEM supplemented with 2% donor equine serum (from Gibco), 1% penicillin/streptomycin and 2 mg/mL<sup>-1</sup> ACA). After 7 additional days, gels were fixed with 4% PFA and cells permeabilized with 0.5 % Triton X-100 for 15 min. After several rinsing with PBS solution, actin filaments were stained with Alexa Fluor 488 phalloidin and nuclei with 4',6'-Diamidino-2-phenylindole (DAPI) solution. Staining of myosin heavy chain in differentiated C2C12 was performed with MF-20 hybridoma mouse IgG2B primary antibody and Alexa Fluor 546 goat anti-mouse IgG2B secondary antibody (Invitrogen). Gels were imaged with a fluorescence microscope (Axio Imager D.1, Zeiss) and processed using Image J software.

Myotube number per field of view (approximately 870\*655 μm, low magnification) was assessed on at least 4 (up to 11) different pictures taken from at least 2 different samples for each type of gel. Myotube density as quantitatively evaluated by the ratio of total myotube area was

done using thresholded images based on myosin staining, and was assessed on least 3 (up to 6) different pictures taken from at least 2 different samples for each type of gel. Length of individual myotubes was evaluated either manually or, whenever possible, by means of maximum Feret diameter analysis. Width of individual myotubes was evaluated either manually or by using the most relevant option between minimum Feret diameter analysis or minor axis measurement (Fit ellipse). At least 11 (up to 49) myotubes on at least 4 (up to 11) different pictures taken from at least 2 different samples were considered for each type of gel.

**Statistical Analysis.** Data were submitted to analysis of variance (ANOVA), and means were compared using the test of Tukey. Different letters correspond to statistically-different values ( $P < 0.05$ ). \* represents statistically-different levels. \* means  $P$ -value  $< 0.05$ ; \*\* means  $P$ -value  $< 0.01$ ; \*\*\* means  $P$ -value  $< 0.001$ .

## Results

**Fibrinogen-CNC Interactions in Diluted Conditions.** In a first step, we investigated the interactions between CNC and fibrinogen molecules in suspensions. All studies were performed in the same buffer (20 mM sodium citrate-HCl, pH 7.2) as the one used later to form composite hydrogels. Diluted conditions were studied to limit CNC particles aggregation. However, depending on the considered techniques, minimum concentrations required to obtain reliable measurements could vary from  $0.025 \text{ mg.mL}^{-1}$  to  $0.5 \text{ mg.mL}^{-1}$ . In parallel the range of fibrinogen:CNC weight ratio was kept similar in all experiments and did not exceed 2.5:1.

The ability of fibrinogen to interact with CNCs was first studied by DLS (**Figure 1(a)**). At a concentration of  $0.025 \text{ mg.mL}^{-1}$ , the apparent hydrodynamic diameter of CNC nanoparticles was  $165 \pm 25 \text{ nm}$ . Upon successive addition of fibrinogen solutions at  $0.050 \text{ mg.mL}^{-1}$ , the apparent

hydrodynamic diameter first increased up to  $230 \pm 40$  nm for a Fbg:CNC ratio of 0.20:1. Then an apparent plateau was observed up to Fbg:CNC = 0.32:1. Above this ratio, the apparent hydrodynamic diameter rose again up to *ca.* 350 nm and then appeared to slowly increase with additional fibrinogen amount. No measurable difference in the viscosity were obtained for these suspensions, in agreement with the highly diluted conditions. Determination of the precise Fbg:CNC ratio where the second increase stops is not possible due to the measurement error ( $\pm 60$  nm) but from Fbg:CNC = 0.50:1 and above, the distribution of hydrodynamic diameter values does not overlap anymore with that of Fbg:CNC = 0.32:1. It is also important to point out that, although the error range increased with Fbg:CNC ratio, it was always smaller than  $\pm 80$  nm, indicating that well-defined nanoscale objects were present in the mixture. This correlates with the macroscopically-observed colloidal stability of these suspensions. To support these observations, the scattering intensity of a Fbg:CNC 1:1 suspension was recorded and found stable over *ca.* 2 h before it started to decrease slowly (Supporting Information, **Figure S1**). Finally, in the fibrinogen concentration range of these experiments, the protein-only solutions did not yield to a measurable signal, suggesting that only CNC or CNC-Fbg assemblies contributed to the monitored hydrodynamic diameters.

Zeta potential ( $\zeta$ ) measurements were then performed using  $0.25 \text{ mg.mL}^{-1}$  CNC suspensions and  $0.50 \text{ mg.mL}^{-1}$  Fbg solutions. In such conditions,  $\zeta$  values could be measured for both components, *i.e.*  $-28 \pm 6$  mV for cellulose nanocrystals and  $-7 \pm 5$  mV for fibrinogen. Upon successive addition of Fbg to CNC, the average  $\zeta$  value increased up - 19 mV for a Fbg:CNC ratio of 0.20:1 and then remained constant (**Figure 1(b)**). On the one hand, the error range, which was comparable to the  $\zeta$  value of Fbg, did not allow to conclude on the significance of these variations. On the other hand, one should notice that the apparent ratio for which the average  $\zeta$  value reached

a maximum corresponds to the ratio where a first plateau was reached in DLS experiments. Moreover, the error range never exceeded  $\pm 7$  mV, which is again in favor of the formation of well-defined objects rather than uncontrolled aggregation.

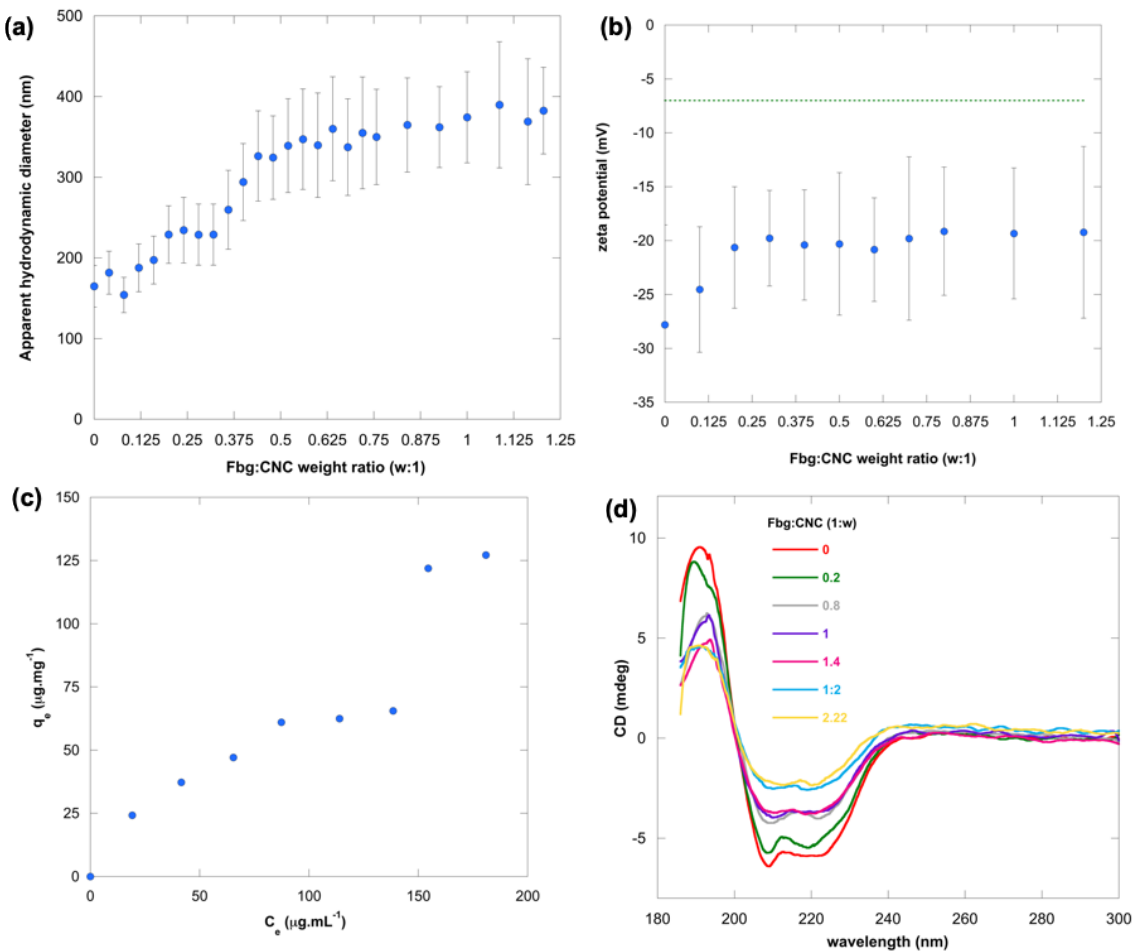


Figure 1. Characterization of diluted solutions and suspensions of Fbg, CNC and Fbg-CNC mixtures in citrate buffer. (a) Evolution of apparent hydrodynamic diameter, as obtained from DLS, at fixed initial CNC concentration ( $0.25 \text{ mg}\cdot\text{mL}^{-1}$ ) and variable Fbg:CNC weight ratio. (b) Evolution of Zeta potential at fixed initial CNC concentration ( $0.25 \text{ mg}\cdot\text{mL}^{-1}$ ) and variable Fbg:CNC weight ratio (dashed green light indicates the zeta potential of pure fibrinogen). (c) Adsorption isotherm of fibrinogen on CNC ( $C_e = \text{Fbg concentration at equilibrium}$ ,  $q_e = \mu\text{g}$  of adsorbed Fbg per mg of CNC). (d) Evolution of CD spectra at fixed Fbg concentration and variable Fbg:CNC weight ratio.

To obtain more quantitative data on the putative adsorption of fibrinogen on cellulose nanocrystals, sorption isotherms were performed using the BCA method to determine the concentration of free protein in solution. A preliminary calibration curve showed a linear relationship between Fbg concentration and absorbance at  $\lambda = 562$  nm in the 10-500  $\mu\text{g}\cdot\text{mL}^{-1}$  range (Supporting Information, **Figure S2**). The calculated isotherm evidenced a two-step process (**Figure 1(c)**). The amount of adsorbed fibrinogen first increased up to *ca.* 60  $\mu\text{g}$  of Fbg per mg of CNC. A plateau was observed and then the amount of adsorbed proteins increased again, reaching *ca.* 125  $\mu\text{g}\cdot\text{mg}^{-1}$ , *i.e.* twice the value at the first plateau. Altogether, these data confirm that fibrinogen interacts with cellulose nanocrystals in two well-defined successive steps.

To obtain further evidence of fibrinogen adsorption, CD measurements were performed on Fbg solutions with various added volumes of CNC. Representative spectra are shown on **Figure 1(d)** and spectra for all samples are provided as Supporting Information, **Figure S3**. The CD spectrum of pure Fbg shows three main bands, one positive peak ( $I_1$  at 190 nm) and two negative signals ( $I_2$  at 209 nm and  $I_3$  at 220 nm), in agreement with the literature.<sup>46</sup> As the volume of the CNC suspension increased, the intensity of the  $I_1$  band decreased. Such a decrease was also observed when equivalent volumes of citrate buffer were added, suggesting that it reflects the dilution of the protein (Supporting Information, **Figure S4**). However, the relative intensity of the  $I_2$  and  $I_3$  peaks also varied with CNC suspension volume, such a variation being not observed when only buffer was added. In more details,  $I_2$  was more intense than  $I_3$  for pure Fbg and remained so until Fbg:CNC ratio 0.7:1. Above this ratio, the two peaks were of comparable intensity, indicating a conformational change of Fbg that should originate from its interaction with CNC. For each condition, the CD spectrum is the sum of adsorbed and free fibrinogen spectra so that the above-

mentioned ratio should correspond to conditions where adsorbed Fbg molecules prevail over those remaining in solution.

Selected conditions were further studied by Small Angle X-Ray Scattering. Reference spectra for pure fibrinogen solutions exhibited similar shape and increasing intensity with increasing protein content (Supporting Information, **Figure S5**). In sharp contrast, the curves for CNC suspensions ( $4 \text{ mg.mL}^{-1}$ ) as such or mixed with increasing amounts of fibrinogen were very similar both in shape and intensity (**Figure 2(a)**). On the one hand, the absence of significant modification of intensity at low  $q$  values and of the slope at intermediate  $q$  confirms the absence of extensive aggregation of the CNC, as already suggested by DLS. On the other hand, the limited variations at high  $q$  suggest that fibrinogen molecules, if adsorbed on CNC particles, do not form a dense layer.

Selected suspensions were also studied by rheology under steady shear (**Figure 2(b)**). For pure fibrinogen solutions, apparent viscosity  $\eta$  values did not significantly vary with Fbg concentration in the  $0.125\text{-}0.500 \text{ mg.mL}^{-1}$  range and the log-log plot of  $\eta$  vs shear rate evidenced a linear decrease from  $100 \text{ Pa.s}$  to  $0.001 \text{ Pa.s}$ , following a Power law model. In contrast, for a CNC suspension at  $0.250 \text{ mg.mL}^{-1}$ , the linearity domain was observed up to a shear rate of *ca.*  $100 \text{ s}^{-1}$  followed by a smoother decrease and viscosity values were one order of magnitude lower than for Fbg in the linear region. Such a shear thinning behaviour reflects the ability of CNCs to orientate under the shearing flow at high rate. For 1:2 Fbg:CNC ratio, the evolution was similar to CNC alone but viscosity values were slightly larger. For the 1:1 ratio, viscosity values were similar to those of pure CNC at low shear rates. However, a plateau was evidenced in the  $10\text{-}30 \text{ s}^{-1}$  shear rate domain and then viscosity values became close to those of pure fibrinogen. For the 2:1 Fbg:CNC composition, a similar transition from a CNC-like behavior at low shear rates to a Fbg-like

behaviour at higher shear rates was also observed but it occurs at a lower shear rate (*ca.*  $1 \text{ s}^{-1}$ ) and more progressively. Taken together, it would suggest that, above a certain ratio, the presence of Fbg favors the alignment of CNC particles under the shearing flow. Moreover, once such an alignment has occurred, CNCs do not contribute significantly to the viscosity of the suspension, which is mainly determined by the protein content.

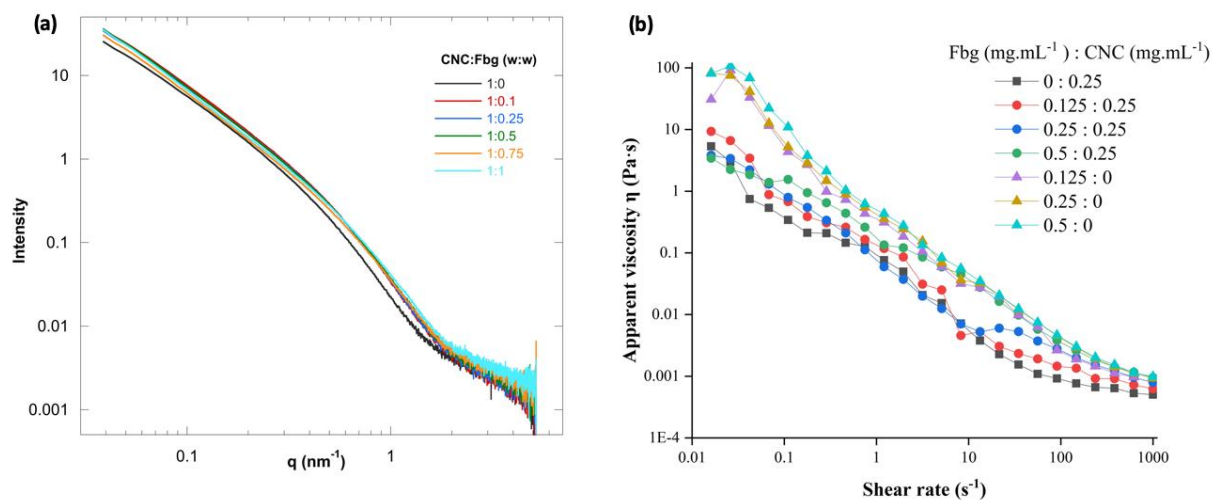


Figure 2. (a) SAXS spectra of pure CNC ( $4 \text{ mg.mL}^{-1}$ ) and different CNC-fibrinogen mixtures, (b) Apparent viscosity as determined under steady shear for pure CNC (square), pure fibrinogen (triangles) and fibrinogen:CNC mixtures (circles)

Suspensions prepared with similar ratio were observed by cryo-TEM. In pure Fbg samples, fibrinogen molecules were difficult to observe individually due to the concentration and equipment limitations (Supporting Information, **Figure S6**). Suspensions of pure CNC showed needles  $135 \pm 20 \text{ nm}$  in length, in good agreement with the value obtained from DLS on pure CNC particles ( $165 \pm 25 \text{ nm}$ ) (**Figure 3(a)**). It was noticed that these particles tended to be located on the TEM grid or at the interface between the grid and the frozen water rather than inside the grid holes. For the Fbg:CNC 1:2 (w:w) samples, cellulose nanocrystals were observed as isolated needles or as star-



like patterns (**Figure 3(b)**). No clear modification in CNC organization could be observed for a 1:1 ratio (**Figure 3(c)**). Finally, for the highest Fbg relative content, linear assemblies of CNC could be frequently observed (**Figure 3(d)**). Such an ability of fibrinogen to favor the co-alignment of CNCs may be correlated to the above-observed decrease of the shear rate value required to reach the viscosity plateau in mixed suspensions.

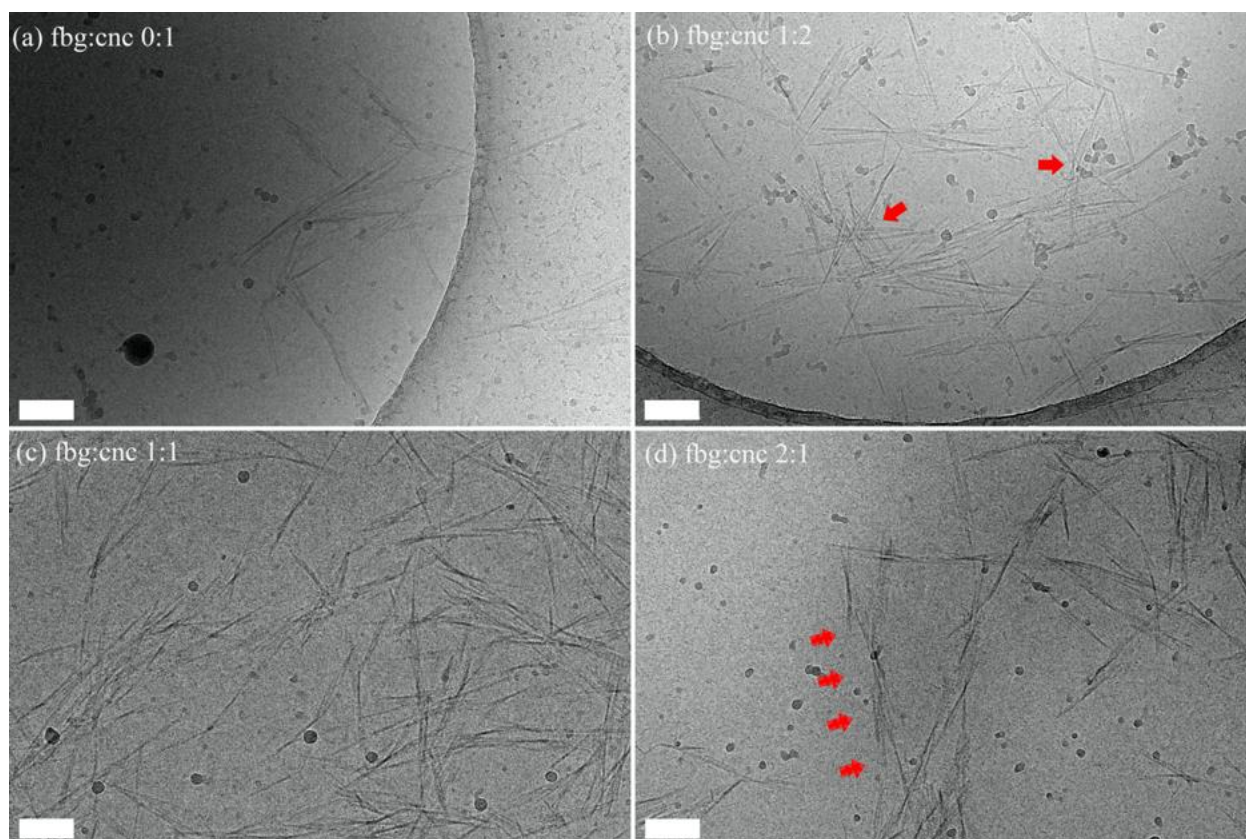


Figure 3. Cryo-TEM images of (a) pure CNC and Fbg-CNC mixtures at Fbg:CNC weight ratio of (b) 1:2, (c) 1:1 and (d) 2:1 (scale bar = 100 nm). Red arrows highlight star-like (b) and aligned (d) patterns of CNCs

**Fibrin-CNC Hydrogels.** In a second step, fibrin-CNC hydrogels were prepared by mixing fibrinogen and cellulose nanocrystals in citrate buffer and then adding thrombin to trigger fibrin formation, fibrillogenesis and gel formation. Initial fibrinogen concentrations of  $20 \text{ mg}\cdot\text{mL}^{-1}$  and

30 mg.mL<sup>-1</sup> were fixed as a compromise between high content to maximize mechanical properties of the gels and low content to obtain homogeneous suspensions with a measurable lag time (*i.e.* delay between thrombin addition and gel formation). For CNC suspensions, a maximum concentration of 30 mg.mL<sup>-1</sup> could be achieved while the suspension remained homogeneous and with practical viscosity. Mixtures were obtained by adding 100 μL of CNC to 900 μL of fibrinogen so that the final CNC concentration was 3 mg.mL<sup>-1</sup> and therefore the maximal Fbg:CNC ratio was *ca.* 10:1 (w:w).

The kinetics of fibrillogenesis was followed by monitoring absorbance at  $\lambda = 400$  nm, *i.e.* turbidimetry measurements, at 25°C. As shown on **Figure 4(a)**, the pure Fbg solution at 20 mg.mL<sup>-1</sup> supplemented with 100 μL citrate buffer has an initial low absorbance which, after thrombin addition, increases after 1 min and stabilizes at *ca.* 2.7 after 30 min. When a 5 mg.mL<sup>-1</sup> CNC suspension was added, the initial absorbance was *ca.* 0.8 and increased as soon as thrombin was added. Such an increase was slower than in the absence of CNC and absorbance reached *ca.* 2.2 after 30 min but without a plateau. For other conditions, the initial absorbance systematically increased with CNC content. Thrombin addition led to a small increase of absorbance which then only moderately evolve, or even remained constant for the highest CNC concentration. Absorbance after 30 min also increased with initial cellulose nanocrystals content but remained smaller than that of pure fibrinogen. Control experiments performed without fibrinogen indicated that the absorbance of CNC suspensions increased with concentration but was always smaller than that of fibrinogen-CNC mixtures, and did not evolve with time (Supplementary Information, **Figure S7**). For a 30 mg.mL<sup>-1</sup> fibrinogen concentration, the initial absorbance was slightly higher than for the 20 mg.mL<sup>-1</sup> and the increase of absorbance occurred immediately after thrombin addition (**Figure 4(b)**). In the presence of CNCs, initial absorbance values were also systematically

higher than at 20 mg.mL<sup>-1</sup> and increased with CNC concentration. In terms of kinetics, the lowest CNC content preserved the initial fast increase in absorbance and observation of a plateau. For higher CNC contents, a similar trend as for the 20 mg.mL<sup>-1</sup> fibrin gels was observed but with a shift in the effect of nanocrystals concentration, *i.e.* the 20 mg.mL<sup>-1</sup> CNC suspension added to the 30 mg.mL<sup>-1</sup> Fbg solution had a similar effect as the 10 mg.mL<sup>-1</sup> CNC suspension added to the 20 mg.mL<sup>-1</sup> Fbg solution. It can however be noticed that, in these conditions, the final absorbance values decreased with increasing CNC content and were much closer to that of the pure 30 mg.mL<sup>-1</sup> fibrin hydrogel. Altogether, the presence of CNCs does have a clear, apparently inhibitory effect on fibrillogenesis and the extent of such an effect depends both Fbg concentration and Fbg:CNC ratio.

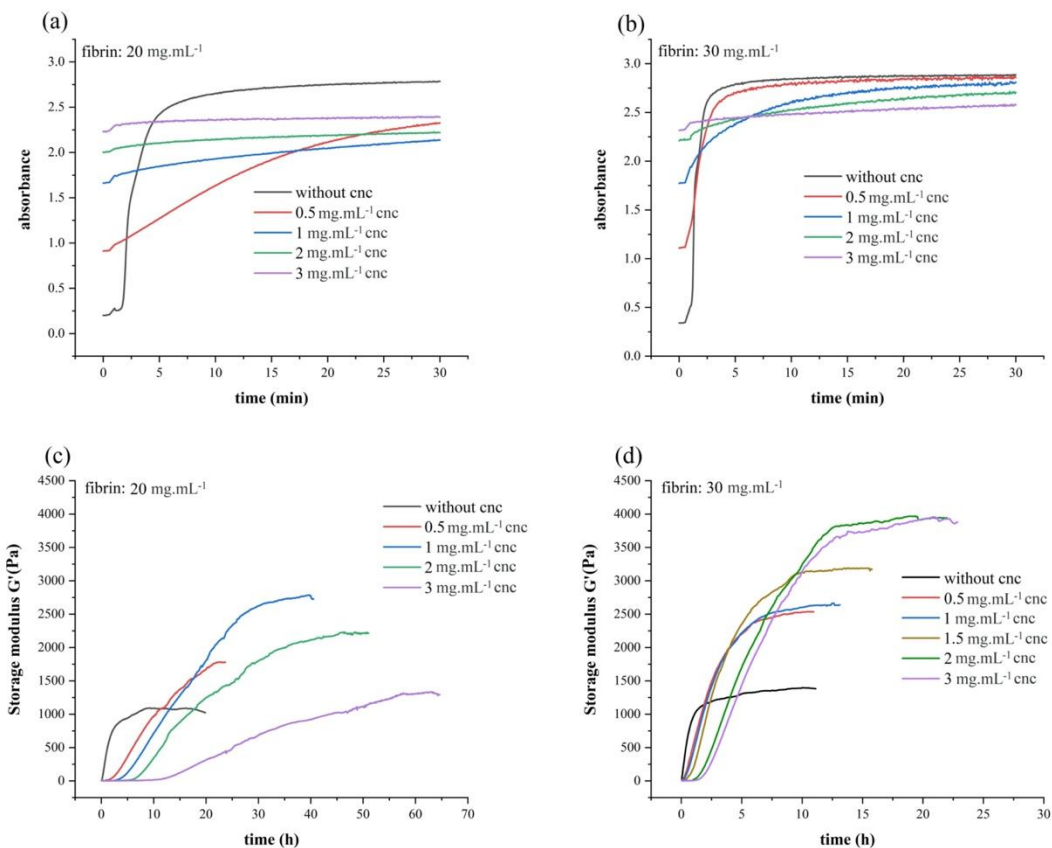


Figure 4. Time evolution of (a,b) absorbance at  $\lambda = 400$  nm and (c,d) storage modulus of fibrinogen solutions at (a,c) 20 mg.mL<sup>-1</sup> and (b,d) 30 mg.mL<sup>-1</sup>) after addition of CNC suspensions (0.5-3 mg.mL<sup>-1</sup> final concentration) and thrombin. Dark lines correspond to pure fibrinogen solutions after thrombin addition

The same mixtures were further studied by rheological measurements at 37°C, which were run until a plateau in storage modulus  $G'$  value was reached. For the pure fibrin gel at 20 mg.mL<sup>-1</sup>,  $G'$  increased steeply for *ca.* 2h and then more smoothly until a plateau was reached after 10 h, reaching a maximum value of 1.1 kPa (**Figure 4(c)**). In the presence of 0.5 mg.mL<sup>-1</sup> CNC, the increase was slightly delayed and slower and the  $G'$  value stabilized after 22 h at 1.75 kPa. Increasing further CNC concentration extended the initial delay, slowed down the  $G'$  increase rate and lengthened the time required to reach the plateau. However, while the presence of 1 mg.mL<sup>-1</sup> CNC led to a maximum  $G'$  value of 2.8 kPa, *i.e.* more than twice that of the pure fibrinogen solution, larger cellulose content resulted in a progressive decrease of the storage modulus value at the plateau, which nevertheless remained superior to that of pure fibrinogen. Pure fibrin solutions at 30 mg.mL<sup>-1</sup> showed a quite similar behavior as 20 mg.mL<sup>-1</sup> ones, with a comparable maximal  $G'$  value (1.4 kPa) but a shorter delay required to reach the  $G'$  plateau (**Figure 4(d)**). The presence of 0.5 mg.mL<sup>-1</sup> and 1.0 mg.mL<sup>-1</sup> CNC slightly slowed down  $G'$  evolution but the final value significantly increased (*ca.* 2.5 kPa). The presence of 2 mg.mL<sup>-1</sup> and 3 mg.mL<sup>-1</sup> CNC delayed further the increase in  $G'$  but the maximal values were also larger, reaching *ca.* 4 kPa. To confirm this evolution, an additional composition was studied (1.5 mg.mL<sup>-1</sup>) resulting in an intermediate  $G'$  value between those of the 1 mg.mL<sup>-1</sup> and 2 mg.mL<sup>-1</sup> composites.

Structure of the hydrogels was investigated by TEM. For pure fibrin gels at 20 mg.mL<sup>-1</sup>, large fibers, several microns in length and up to *ca.* 200 nm in width were observed (**Figure 5(a)**). In the presence of 1 mg.mL<sup>-1</sup> CNC, a dramatical decrease in fibrin fiber size was seen, especially in width that was below 100 nm (**Figure 5(b)**). At 2 mg.mL<sup>-1</sup> CNC, even smaller fibers were

observed (**Figure 5(c)**). A similar evolution was observed for gels at 30 mg.mL<sup>-1</sup> fibrin concentration (**Figure 5(d-g)**). Moreover, as the size of fibrin fibers decreases with increasing CNC content, they seem to form aggregates of increasing size. Higher magnification images clearly evidence the change from large fibers in pure fibrin gels (**Figure 5(h)**) to small and thin aggregated ones in the presence of 3 mg.mL<sup>-1</sup> CNC (**Figure 5(i)**). Moreover, for the latter samples, CNC needles could be visualized within the fibrin aggregates. However, it was not possible to draw any conclusion on CNC organization, and especially on their possible alignment, within the hydrogels.

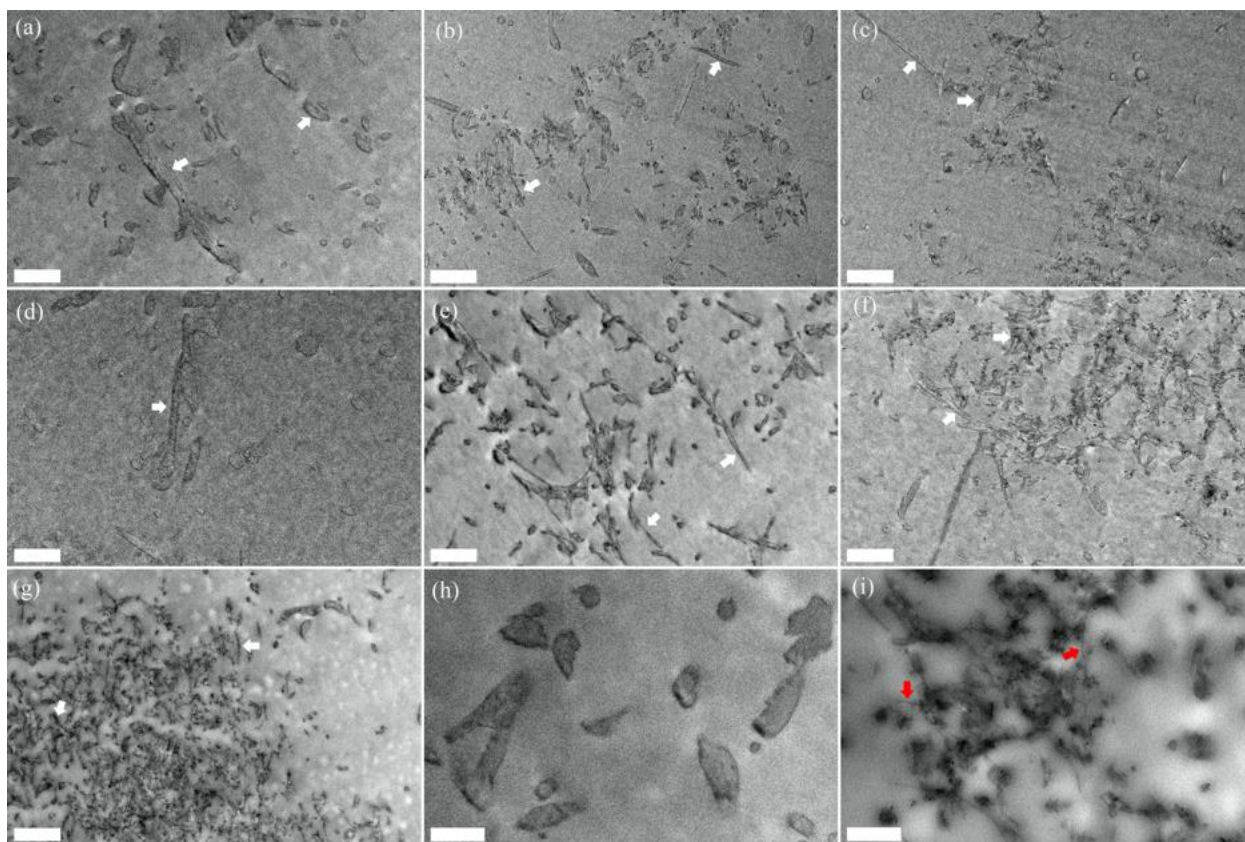


Figure 5. TEM images of fibrin and fibrin-CNC hydrogels (a) pure fibrin at 20 mg.mL<sup>-1</sup>, (b) fibrin 20 mg.mL<sup>-1</sup>: cnc 1 mg.mL<sup>-1</sup>, (c) fibrin 20 mg.mL<sup>-1</sup>: cnc 2 mg.mL<sup>-1</sup>; (d) pure fibrin at 30 mg.mL<sup>-1</sup>, (e) fibrin 30 mg.mL<sup>-1</sup>: cnc 1 mg.mL<sup>-1</sup>, (f) fibrin 30 mg.mL<sup>-1</sup>: cnc 2 mg.mL<sup>-1</sup>; (g) fibrin 30 mg.mL<sup>-1</sup>: cnc 3 mg.mL<sup>-1</sup> (scaler bar = 1  $\mu$ m). Higher magnification

images of (h) pure fibrin at 30 mg.mL<sup>-1</sup>, (i) fibrin 30 mg.mL<sup>-1</sup>: cnc 3 mg.mL<sup>-1</sup> (scale bar = 500 nm). White arrows (a-g) highlight fibrin fibers and red arrows (i) point towards CNCs.

The possibility to use fibrin-CNCs hydrogels as 2D substrates for muscular cells growth and differentiation was finally studied. C2C12 cells were first deposited on fibrin and composite hydrogels in a DMEM medium supplemented with 10 % fetal bovine serum. Proliferation was followed by Alamar Blue test (**Figure 6**). On all gels a slow increase of cell population during 4 days was observed followed by an acceleration of cell metabolism. No difference in cell growth was observed between pure 20 mg.mL<sup>-1</sup> and 30 mg.mL<sup>-1</sup> hydrogels. A significant increase in proliferation was noticed when 0.5 mg.mL<sup>-1</sup> CNC were present within 20 mg.mL<sup>-1</sup> gels but further cellulose nanocrystal addition did not lead to further improvement. In contrast, the presence of CNC within 30 mg.mL<sup>-1</sup> gels did not induce any modification of C2C12 cells proliferation.

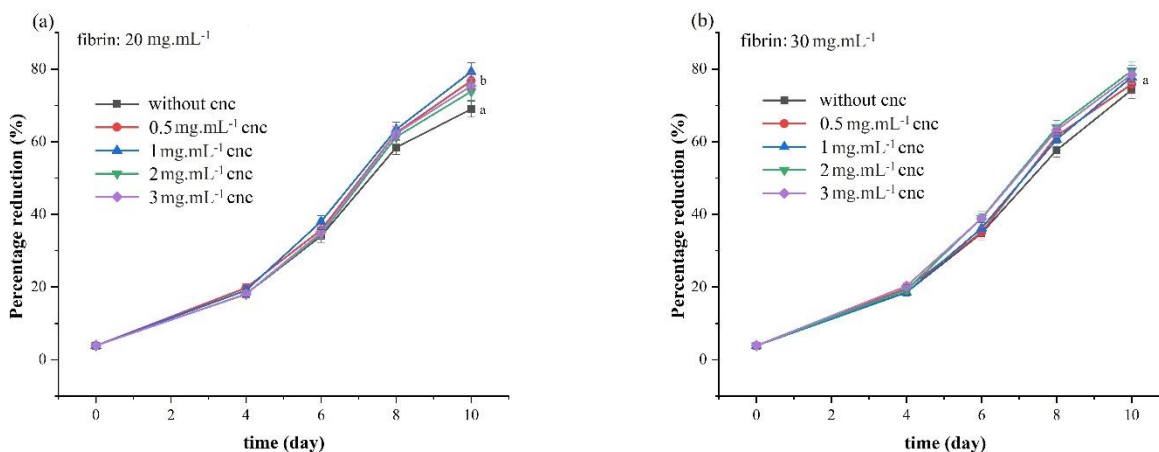


Figure 6. Evolution of C2C12 proliferation on fibrin-CNC composite gels as monitored by Alamar Blue test (a) fibrin 20 mg.mL<sup>-1</sup>; (b) fibrin 30 mg.mL<sup>-1</sup>. Different letters correspond to statistically-different values ( $P < 0.05$ ).

The ability of the different hydrogels to favor C2C12 differentiation was then studied. For this purpose, cells were cultured for 4 days in a serum-rich DMEM medium as previously

described and then for 7 additional days in a low serum (2% donor equine serum)-DMEM medium. Almost all substrates displayed very high cell densities as evidenced by phalloidin labeling with clear formation of myotubes as evidenced by MF20 positive staining (**Figure 7**). The only exception was the fibrin 20 mg.mL<sup>-1</sup> - CNC 3 mg.mL<sup>-1</sup> hydrogels where little cell adhesion was observed (Supporting Information, **Figure S8**).

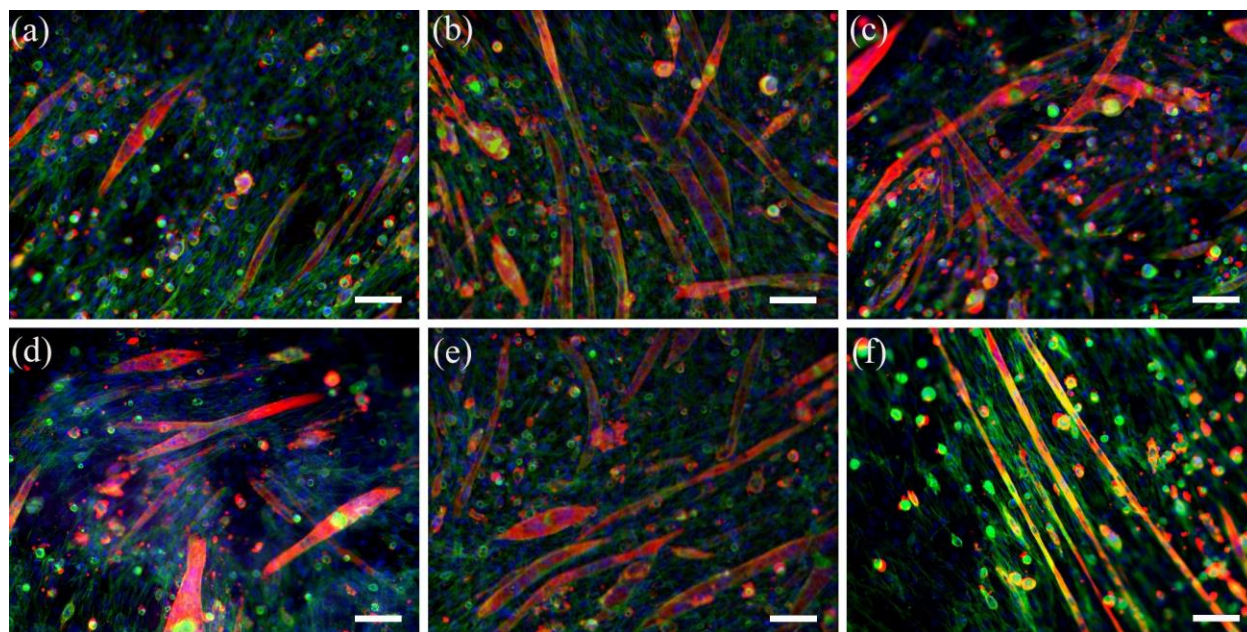


Figure 7. Fluorescence images of C2C12 cells cultured for 4 days in serum-rich and 7 days in low-serum DMEM within (a) pure fibrin at 20 mg.mL<sup>-1</sup>, (b) fibrin 20 mg.mL<sup>-1</sup>: CNC 1 mg.mL<sup>-1</sup>, (c) fibrin 20 mg.mL<sup>-1</sup>: CNC 2 mg.mL<sup>-1</sup>; (d) pure fibrin at 30 mg.mL<sup>-1</sup>, (e) fibrin 30 mg.mL<sup>-1</sup>: CNC 1 mg.mL<sup>-1</sup>, (f) fibrin 30 mg.mL<sup>-1</sup> : CNC 3 mg.mL<sup>-1</sup>. (Blue: DAPI, green: actin, red: MF20). Scale bar = 100  $\mu$ m.

Quantitative analysis evidenced that myotube number and total myotube area are much higher on pure fibrin gels at 30 mg.mL<sup>-1</sup> compared to pure fibrin at 20 mg.mL<sup>-1</sup> (**Figure 8**). For the gels at 30 mg.mL<sup>-1</sup> there is no significant change in myotube number and density upon CNCs addition, whereas for the gels at 20 mg.mL<sup>-1</sup> myotube number significantly increases upon CNCs addition for the concentrations up to 1 mg.mL<sup>-1</sup>, and tends to decrease from 1 to 2 mg.mL<sup>-1</sup>.

Myotube density also tends to display a peak around 1 mg.mL<sup>-1</sup> CNC although the variation was not statistically significant. For both considered parameters, the values corresponding to the maxima at 20 mg.mL<sup>-1</sup> fibrin-1 mg.mL<sup>-1</sup> CNC are similar to those on 30 mg.mL<sup>-1</sup> at any CNC concentration.

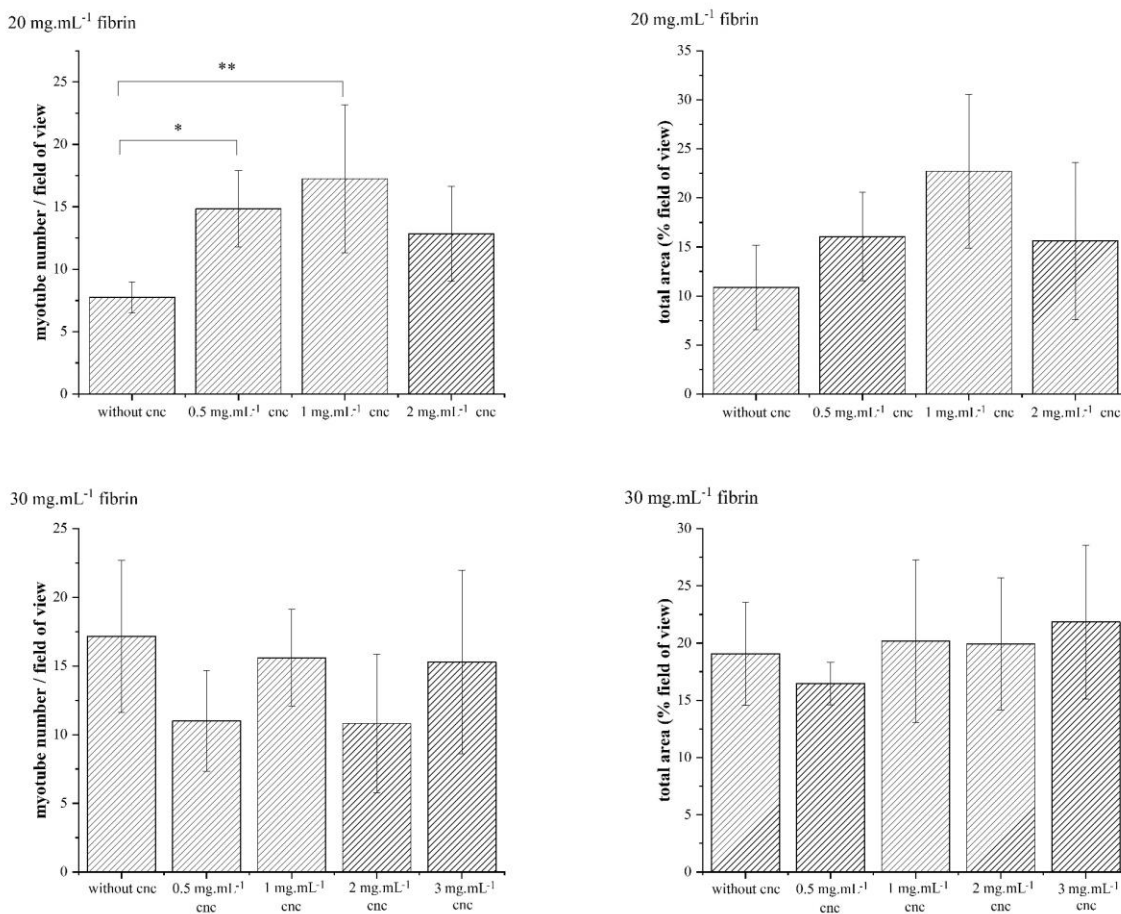


Figure 8. Average myotube number per field of view and relative substrate area covered by myotubes, depending on substrate type.

Analysis of individual myotubes morphology on pure fibrin gels at 20 mg.mL<sup>-1</sup> and 30 mg.mL<sup>-1</sup> reveals no strong difference regarding length and width average values (**Figure 9**). Still, the highest length value is about 530  $\mu$ m at 20 mg.mL<sup>-1</sup> (N=11) (**Figure 9(a)**) whereas at 30 mg.mL<sup>-1</sup> 25% of the myotubes present a length range between 550 and 1250  $\mu$ m (N=34) (**Figure**



**9(b)**). Upon addition of CNC in 20 mg.mL<sup>-1</sup> fibrin gels myotube length tends to increase with a significant difference between pure fibrin and composite hydrogel with 2 mg.mL<sup>-1</sup> CNC (**Figure 9(a)**). On these composite hydrogels myotube width reduction is observed, with a significant difference between pure fibrin and composite hydrogel with 1 and 2 mg.mL<sup>-1</sup> CNC. For the 30 mg.mL<sup>-1</sup> fibrin-based composite gels, morphology analysis also reveals longer and thinner myotube distribution upon increasing CNC concentration (as already observed on **Fig. 7(f)**). The difference regarding observed length values is highly significant between 30 mg.mL<sup>-1</sup> fibrin-3 mg.mL<sup>-1</sup> CNC and every other type of 30 mg.mL<sup>-1</sup> fibrin-based gels (**Fig. 9(c)**). The width values decrease in 30 mg.mL<sup>-1</sup> fibrin-based gels is more generally observed upon CNCs addition, with multiple significant differences between the different types of gels (**Fig. 9(d)**). Noteworthy myotubes longer than 1 mm can be observed on almost every type of fibrin-CNC composite hydrogels. In particular, on the fibrin 20 mg.mL<sup>-1</sup>-CNC 2 mg.mL<sup>-1</sup> composite hydrogels 25% of the myotubes are longer than 800 μm (N= 24), and on fibrin 30 mg.mL<sup>-1</sup>-3 mg.mL<sup>-1</sup> hydrogels (N= 25), 25% of the myotubes are longer than 880 μm (with respective maximal values of approximately 1100 μm and 1600 μm).

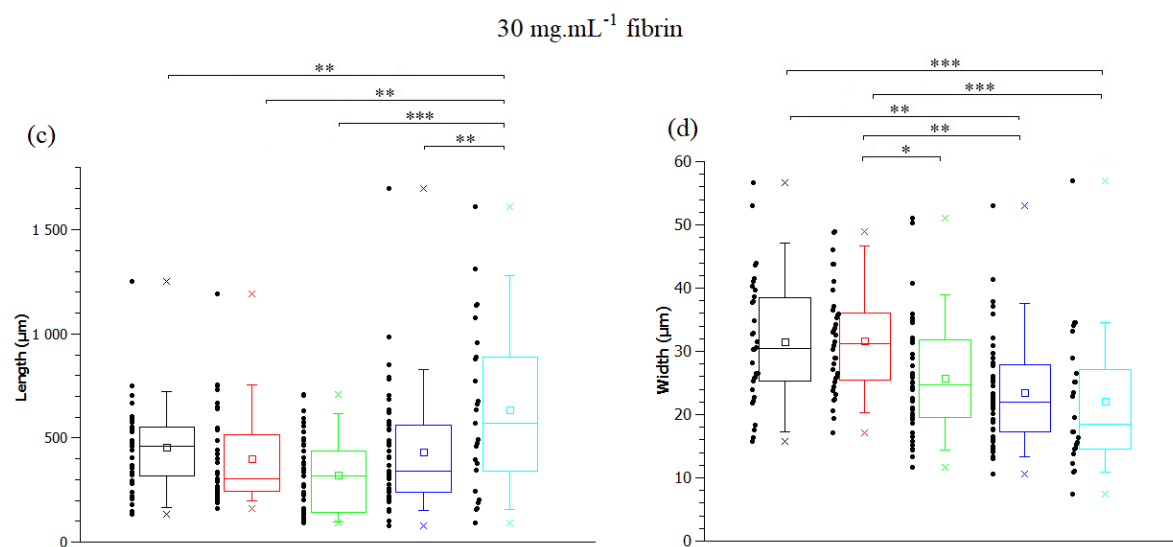
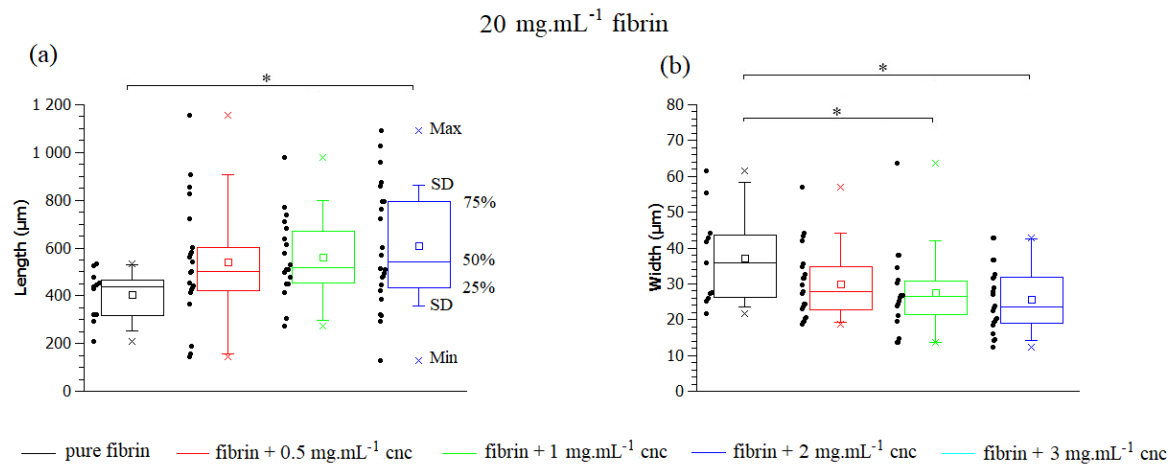


Figure 9. Boxplot analysis of myotube morphological parameters depending on substrate type. Every displayed bullet on the left-hand side of the boxplots represents an actual data. Black: pure fibrin; red: fibrin + 0.5 mg.mL<sup>-1</sup> CNC; green: fibrin + 1 mg.mL<sup>-1</sup> CNC; purple: fibrin + 2 mg.mL<sup>-1</sup> CNC; light blue: fibrin + 3 mg.mL<sup>-1</sup> CNC (for 30 mg.mL<sup>-1</sup> fibrin gels only).

## Discussion

Properties of nanocomposites are strongly dependent of interactions between fillers and matrix. Therefore, in a first step we investigated the interactions of fibrinogen with CNC in diluted conditions. The medium selected for this study was the citrate buffer (citrate-HCl, 20 mM citrate, pH 7.2) used afterwards to form hydrogels. It insures near neutral pH conditions where both fibrinogen, whose reported isoelectric point is ca. 5.5,<sup>47</sup> and CNC, that bears sulfonate surface groups resulting from the sulfuric acid treatment,<sup>48</sup> are expected to be negatively-charged, as confirmed by measured  $\zeta$  values.

Upon addition of increasing amounts of fibrinogen to CNC, an increase in apparent hydrodynamic diameter was measured. Such an increase occurred in two steps and could be correlated to fibrinogen adsorption by the isotherm established by titration of free proteins using the BCA technique. Zeta potential measurements also suggested that fibrinogen adsorption occurred as  $\zeta$  values increased upon initial fibrinogen addition as a result of the higher  $\zeta$  value of the protein compared to that of CNC. However, the small difference between these two values and the relatively high error range of measurements did not allow to fully conclude on this point nor to confirm the two-step process. Meanwhile, Cryo-TEM evidenced that presence of low amount of fibrinogen leads to the formation of some star-shaped aggregates while higher amounts induced local linear organizations of CNCs. It is important to point out that, for rod-like particles, application of the Stokes-Einstein relation to DLS data leads to an apparent hydrodynamic diameter only, corresponding to a sphere whose diameter is equivalent to the rod length.<sup>49</sup> Thus, the increase in apparent hydrodynamic parameter could correlate well with the local formation of linear CNC aggregates but provides no information on the width of these aggregates, as long as it remains significantly smaller than their width. In this context, SAXS measurements confirm the absence of wider aggregates.<sup>50</sup> However, the presence of linear aggregates could not be evidenced

by this technique as the expected repetition motif would correspond to a CNC particle length, *ca.* 150-200 nm, that would lie in a  $q$  value range much smaller than the one investigated here.

Viscosity measurements provide additional information. Fibrinogen solutions show a shear-thinning behavior while pure CNC suspension exhibited a two-step regime, both agreeing with the literature.<sup>51,52</sup> This two-step regime corresponds to the increased orientation of CNC particles with increasing shear rate until maximal alignment is achieved. The resulting apparent viscosity is then close to that of pure water and is constant upon further shear rate increase. Upon fibrinogen addition to CNC, this plateau still appears but as an intermediate regime between a CNC-like behavior and a fibrinogen-like one and at a shear rate that decreases with increasing protein concentration. This suggests that fibrinogen favors CNC alignment and that, once all nanocrystals are aligned, the viscosity of the mixture is determined by its protein content. It is important to point out that the viscosity at high shear rate of the Fbg:CNC 0.5:0.25 (w:w) mixture is very close to that of the pure fibrinogen solution at the same initial concentration, in agreement with the moderate sorption capacity (*ca.* 10 wt%) of CNC towards fibrinogen.

Interactions between fibrinogen and CNC are expected to be weak. Both colloids being negatively charged in the conditions of adsorption, repulsive electrostatic interactions are expected, all the more as the ionic strength is low.<sup>53</sup> Thus, hydrogen bonds and Van der Waals interaction must be responsible for protein adsorption that is therefore mainly energetically-driven by entropy, as reported in the literature.<sup>54</sup> Also in agreement with previous studies,<sup>55</sup> Isothermal Titration Calorimetry experiments showed that the adsorption process produced low heat rates (*ca.* 2  $\mu$ W-0.5  $\mu$ cal.s<sup>-1</sup>) that were not significantly different from that generated by fibrinogen or CNC dilution (Supporting Information, **Figure S9**). Nevertheless, these interactions were effective enough to induce modification of fibrinogen conformation, as indicated by CD measurements. The

observed variations in the relative intensity of the  $I_2$  and  $I_3$  peaks are reminiscent of those observed for fibrinogen adsorbed on hydrophilic self-assembled monolayers, indicating a surface-induced protein refolding (*i.e.* increase of  $\beta$ -sheet vs.  $\alpha$ -helix ratio).<sup>56</sup> Importantly, such a modification was observed up to a 1:1.4 (*i.e.* 0.7:1) ratio Fbg:CNC ratio situated in the second plateau of the DLS curve. This strongly suggests that the observed two-step adsorption process does not correspond to the formation of a double layer of fibrinogen on the CNC surface. CD data also indicated that beyond a *ca.* 1:1 ratio, free fibrinogen largely prevailed over adsorbed ones whose spectrum was no longer apparent. Thus, it is expected that such mixtures containing an excess of fibrinogen compared to CNC should exhibit a preserved ability to form a gel by fibrillogenesis.

The fact that fibrinogen conformation is modified upon interaction with CNCs can explain the observed variation in fibrillogenesis progress as monitored by turbidimetry measurements. For both fibrin concentrations, increase in turbidity upon thrombin addition was slowed down upon CNC addition and the final absorbance at 400 nm of the composite gels was always smaller than that of pure fibrin gels. This contrasts with a previous report using microdispersed oxidized cellulose showing a similar slowing down of fibrillogenesis but an increase in final absorbance.<sup>57</sup> Importantly, here, the impact of CNCs at a given concentration was more significant for the lowest fibrin concentration (compare 1 mg.mL<sup>-1</sup> CNC blue lines on **Figure 4(a)** and **4(b)**). This can be explained considering that, for a fixed CNC amount, the number of adsorbed fibrinogen molecules is the same in both systems but more free proteins able to form the fibrin network are remaining in the 30 mg.mL<sup>-1</sup> suspension compared to the 20 mg.mL<sup>-1</sup>. However if we assume a 0.1 g.g<sup>-1</sup> sorption capacity of CNC towards fibrinogen, 2 mg of CNC should retain 0.2 mg of fibrinogen, *i.e.* 1 % of the fibrinogen content. Such a low variation is unlikely to account for observed modification of turbidimetry curves. As a matter of fact, TEM images indicate a very strong

decrease of fibrin fiber size in the composite hydrogels, even at the lowest CNC concentration (compare **Figure 5(a)** and **(b)** and **Figure 5(d)** and **(e)**). Noticeably, if such a decrease in fiber size can explain the decrease of the final turbidity of the gel, it is again difficult to attribute it only to the small decrease in available fibrinogen content. Therefore, CNCs should influence fibrin gel formation through an additional manner.

Rheological studies allow for monitoring the evolution of the gels beyond their initial setting. A first information is that, although turbidity measurements have suggested that fibrillogenesis may have been strongly inhibited in the presence of high amounts of CNC, all mixtures ultimately formed a gel with  $G'$  values similar or greater than pure fibrin gels at the same concentration. As a matter of fact, the observed trends in turbidity are well-correlated with the time required to observe the increase in storage modulus and the rate of this increase. As pointed out above, only a small fraction of fibrinogen molecules (*ca.* 1 %) are directly interacting with CNC particles' surface. Thus, the major part of them are still available to react with thrombin, fibrillate and form a hydrogel. However, on the long-term, the maximal  $G'$  values do not reflect these initial processes. Especially, for the 30 mg.mL<sup>-1</sup> fibrin gels and nanocomposites, the highest modulus is obtained for the highest CNC amount whose formation is also the most delayed. To understand this point better, it is interesting to note that, because the fibrinogen molecules are *ca.* 10 times shorter than CNC particles and assuming in first approximation that (i) they have a similar diameter and (2) they have a comparable density, a 20:2 or 30:3 w:w nanocomposite composition corresponds in fact to a *ca.* 1:1 v:v ratio, *i.e.* volume fractions of the two components in these gels are comparable. From this perspective, CNCs occupy a significant fraction of the network and should therefore impact both its structure during fibrin percolation and maturation and contribute significantly to its mechanical behavior, especially in their efficiency to act as reinforcing fillers.

While the latter explains the increase in  $G'$  value with CNC content, the former should be considered further to understand the striking decrease in fiber size. One plausible explanation would lie in a confinement effect: it is possible to consider that fibrillogenesis can occur only in spaces delimited by CNC arrangements. Such a confinement should not only limit the local amount of fibrinogen molecules but also limit fibrin fibril length due to CNC particles acting as physical barriers preventing their extension. Thus, the higher the CNC amount, and therefore the higher their volume fraction, the smaller this space is and the more confined fibrillogenesis is.

The influence of CNC addition on the interaction of fibrin hydrogels with muscle cells was then studied. In proliferation conditions, there is no influence of substrate properties on cell viability as evidenced by Alamar blue test. In contrast, in differentiation conditions, the density of myotubes depends on fibrin concentration as well as on CNC concentration for 20 mg.mL<sup>-1</sup> fibrin-based composite substrates. Myotubes morphological parameters also vary depending on substrate properties. In particular a substantial proportion of myotubes longer than 800  $\mu\text{m}$  is observed following addition of highest values of CNC concentrations, which is a remarkable result for *in vitro* culturing conditions.<sup>58</sup> In particular, achieving  $> 1 \mu\text{m}$  long myotubes from C2C12 cell differentiation often involves surface patterning approaches that were not required here.<sup>59</sup>

On fibrin gels at 20 mg.mL<sup>-1</sup> myotube density values are consistent with gel stiffness variation, the highest storage modulus value at 1 mg.mL<sup>-1</sup> CNC corresponding to the highest myotube number and density. On pure fibrin gels at 30 mg.mL<sup>-1</sup> rheological measurements display a  $G'$  value similar to the one at 20 mg.mL<sup>-1</sup>, but the storage modulus keeps increasing upon CNC addition. The observation of differing values regarding myotube number and density between 20 mg.mL<sup>-1</sup> and 30 mg.mL<sup>-1</sup> pure fibrin gels, and of rather constant values for the same parameters

upon CNC addition to 30 mg.mL<sup>-1</sup> fibrin gels, enables to infer that gel stiffness is not the only factor influencing myotube phenotype.<sup>60</sup>

In particular, gel structure examined by TEM exhibited a decrease in the size of fibrin fibers with increasing CNC content, and simultaneous formation of fibrin aggregates of increasing size. The formation of myotubes relies on the contacts established between the myoblasts necessary for subsequent differentiation and fusion, and therefore depends on cell-based matrix contraction and remodeling.<sup>61</sup> The increase of fibrinogen aggregation of thinner fibers upon addition of CNCs might be detrimental to C2C12 interactions with fibrin, leading to a decrease in their differentiation capability. This structural change might therefore counterbalance the effect of gel stiffness increase in the case of 30 mg.mL<sup>-1</sup> fibrin-based composite hydrogels,<sup>62</sup> and explain poor adhesion of cells on 20 mg.mL<sup>-1</sup> fibrin – 3 mg.mL<sup>-1</sup> CNC gels in differentiation condition.

An additional parameter that might be considered to explain myotube phenotype on composite hydrogels is the ability of fibrinogen to favor co-alignment of CNCs, as evidenced by cryo-TEM, DLS and shear flow experiments. Stacking of CNCs inside the composite hydrogels might thus provide nanopatterning cues for the cells that form myotubes following aligned CNCs. Myotube maturation and orientation have already been shown to be favored by alignment of nanoscaled fibres.<sup>63</sup> In particular, Dugan *et al.* showed that myoblasts could sense surface topography related to spin-coating of CNCs with a high degree of orientation.<sup>64</sup> The obtained myotubes were aligned along the CNCs and presented more elongated shapes when compared to glass control. In this system contact guidance could be induced by features of only 10-20 nm. The presence of aligned CNCs inside the composite gels might thus explain length increase and width decrease of myotubes upon addition of CNCs.



Finally, one interesting outcome of the effect of CNC addition to fibrinogen is that it delays the time necessary to form a stable hydrogel after thrombin addition. Since fibrinogen and thrombin react with each other very rapidly, surgical fibrin glue is usually prepared from two different syringes that are mixed directly in the wound bed.<sup>1</sup> We hypothesized that the presence of CNCs would allow to obtain fibrinogen/thrombin mixtures stable enough to be prepared and extruded before gelation. Preliminary experiments following standard protocols<sup>65</sup> did confirm this hypothesis, demonstrating that fibrinogen-CNC-thrombin mixtures constitute injectable formulations (Supplementary Information, **mov-fbg** and **mov-fbgcnc**)

## Conclusions

This work aimed at designing CNC-reinforced fibrin nanocomposite hydrogels using unmodified cellulose nanocrystals and concentrated fibrinogen solutions with potential applications as biomaterials. Although fibrinogen adsorption on CNC was not electrostatically favored in neutral pH conditions, it did occur in non-negligible amounts (*ca.* 100 mg.g<sup>-1</sup>). One of the most interesting consequence of such an adsorption is that CNCs decrease the viscosity of diluted fibrinogen solutions and that fibrinogen favors the alignment of CNCs under flow. Moreover, although CNCs has a strong influence on fibrin gel formation, both in terms of kinetics and nanostructures, the obtained hydrogels could show an improvement of storage modulus (up to 4-fold) and formation of long myotubes, up to 800 μm. Taken together, these results suggest that CNC-fibrinogen mixtures have a strong potential as injectable formulations for the *in situ* formation of nanocomposite hydrogels favoring muscular tissue regeneration.

## ASSOCIATED CONTENT

**Supporting Information.** Additional Dynamic Light Scattering, Circular Dichroism, Small-Angle X-Ray Scattering, Cryo-Transmission Electron Microscopy, UV-visible absorbance and fluorescence imaging data; BCA titration calibration curve; Isothermal Titration Calorimetry data. Injectability tests. The following files are available free of charge.

Supplementary-data.pdf

mov-fbg.avi

mov-fbgcnc.avi

## AUTHOR INFORMATION

### **Corresponding Author**

Phone: +33-1-44274018; E-mail: thibaud.coradin@sorbonne-universite.fr

### **Author Contributions**

The manuscript was written through contributions of all authors. All authors have given approval to the final version of the manuscript.

### **Funding Sources**

K.W. was funded by a China Scholarship Council PhD grant with additional support from the French state funds managed by the ANR within the Investissements d'Avenir program under reference ANR-11-IDEX-0004-02, and more specifically within the framework of the Cluster of Excellence MATISSE led by Sorbonne Universités.

### **Notes**

The authors declare no competing financial interest.

## ACKNOWLEDGMENT

Funding of KW PhD by China Scholarship Council and Cluster of Excellence MATISSE is acknowledged. Authors thanks the Ile-de-France Region for co-funding the ITC equipment in the framework of RESPORE, the Ile-de-France network of Excellence in Porous Solids. The assistance of F. Gélébart and J. Fresnais (PHENIX, Sorbonne Université) for ITC experiments is acknowledged.

## REFERENCES

- (1) Janmey, P. A.; Winer, J. P.; Weisel, J. W. Fibrin gels and their clinical and bioengineering applications. *J. R. Soc. Interface* **2009**, *6*, 1–10.
- (2) Pieters, M.; Wolberg, A. S. Fibrinogen and fibrin: An illustrated review. *Res. Pract. Thromb. Haemost.* **2019**, *3*, 161-172.
- (3) Weisel, J. W.; Litvinov, R. I. Mechanisms of fibrin polymerization and clinical implications. *Blood* **2013**, *121*, 1712–1719.
- (4) Standeven, K. F.; Carter, A. M.; Grant, P. J.; Weisel, J. W.; Chernysh, I.; Masova, L.; Lord, S. T.; Ariëns, R. A. Functional analysis of fibrin gamma-chain cross-linking by activated factor XIII: determination of a cross-linking pattern that maximizes clot stiffness. *Blood* **2007**, *110*, 902-907.
- (5) Helms, C. C.; Ariëns, R. A.; Uitte de Willige, S.; Standeven, K. F.; Guthold, M. alpha-alpha Cross-Links Increase Fibrin Fiber Elasticity and Stiffness. *Biophys. J.* **2012**, *102*, 168-175.

- (6) Ryan, E. A.; Mockros, L. F.; Weisel, J. W.; Lorand, L. Structural Origins of Fibrin Clot Rheology. *Biophys. J.* **1999**, *77*, 2813-2826.
- (7) Weisel, J.W.; Litvinov, R. I. Fibrin mechanical properties and their structural origins. *Matrix Biol.* **2017**, *60–61*, 110-123.
- (8) Vedakumari, W. S.; Prabu, P.; Sastry, T. P. Chitosan-Fibrin Nanocomposites as Drug Delivering and Wound Healing Materials. *J. Biomed. Nanotechnol.* **2015**, *11*, 657-667.
- (9) Ducret, M., Montembault, A.; Josse, J.; Padeloup, M.; Celle, A.; Benchrih, R.; Mallein-Gerin, F.; Alliot-Licht, B.; David, L.; Farges, J.-C. Design and characterization of a chitosan-enriched fibrin hydrogel for human dental pulp regeneration. *Dent. Mater.* **2019**, *35*, 523-533.
- (10) Mu, Z.; Chen, K.; Yuan, S.; Li, Y.; Huang, Y.; Wang, C.; Zhang, Y.; Liu, W.; Luo, W.; Liang, P.; Li, X.; Song, J.; Ji, P.; Cheng, F.; Wang, H.; Chen T. Gelatin Nanoparticle-Injectable Platelet-Rich Fibrin Double Network Hydrogels with Local Adaptability and Bioactivity for Enhanced Osteogenesis. *Adv. Healthc. Mater.* **2020**, *9*, e1901469.
- (11) Hakam, M. S.; Imani, R.; Abolfathi, N.; Fakhrzadeh, H.; Sharifi, A. M. Evaluation of fibrin-gelatin hydrogel as biopaper for application in skin bioprinting: An in-vitro study. *Biomed. Mater. Engin.* **2016**, *27*, 669-682.
- (12) Rowe, S. L.; Stegemann, J. P. Interpenetrating collagen-fibrin composite matrices with varying protein contents and ratios. *Biomacromolecules* **2006**, *7*, 2942-2948
- (13) Heo, D. N., Hospodiuk, M.; Ozbolat, I. T. Synergistic interplay between human MSCs and HUVECs in 3D spheroids laden in collagen/fibrin hydrogels for bone tissue engineering. *Acta Biomater.* **2019**, *95*, 348-356.

- (14) Nilforoushzadeh, M. A., Sisakht, M. M.; Amirkani, M. A.; Seifalian, A.; Banafshe, H. R.; Verdi, J.; Nouradini, M. Engineered skin graft with stromal vascular fraction cells encapsulated in fibrin-collagen hydrogel: A clinical study for diabetic wound healing. *J.Tissue Eng.Reg. Med.* **2020**, *14*, 424-440.
- (15) Coradin, T. ; Wang, K. ; Law, T.; Trichet, L. Type I Collagen-Fibrin Mixed Hydrogels: Preparation, Properties and Biomedical Applications. *Gels* **2020**, *6*, 36.
- (16) Deepthi, S.; Jayakumar, R. Alginate nanobeads interspersed fibrin network as in situ forming hydrogel for soft tissue engineering. *Bioact. Mater.* **2018**, *3*, 194-200.
- (17) Zhou, H. Z; Xu, H. K. K. The fast release of stem cells from alginate-fibrin microbeads in injectable scaffolds for bone tissue engineering. *Biomaterials* **2011**, *32*, 7503-7513.
- (18) Gazzeri, R.; Galarza, M. Alfieri, A.; Neroni, M.; Roperto, R. Simple Intraoperative Technique for Minor Dural Gap Repair Using Fibrin Glue and Oxidized Cellulose. *World Neurosurg.* **2011**, *76*, 173-175.
- (19) Bacakova, M.; Pajorova, J.; Sopuch, T.; Bacakova, L. Fibrin-Modified Cellulose as a Promising Dressing for Accelerated Wound Healing. *Materials* **2018**, *11*, 2314.
- (20) Brown, E. E.; Zhang, J. W., Laborie, M. P. G. Never-dried bacterial cellulose/fibrin composites: preparation, morphology and mechanical properties. *Cellulose* **2011**, *18*, 631-641.
- (21) Zhang, S.; Li, J.; Chen, S.; Zhang, X.; Ma, J.; He, J. Oxidized cellulose-based hemostatic materials. *Carbohydr. Polym.* **2020**, *230*, 115585.
- (22) Dufresne, A. Nanocellulose: a new ageless bionanomaterial. *Mater. Today* **2013**. *16*, 220-227.

- (23) Grishkewich, N.; Mohammed, N.; Tang, J.; Pam, K. C. Recent advances in the application of cellulose nanocrystals. *Curr. Opin. Colloid Interface Sci.* **2017**, *29*, 32-45.
- (24) De France, K. J.; Hoare, T.; Cranston, E. D. Review of Hydrogels and Aerogels Containing Nanocellulose. *Chem. Mater.* **2017**, *29*, 4609-4631.
- (25) Thomas, B.; Raj, M. C.; B, A. K.; H, R. M.; Joy, J.; Moores, A.; Dirsko, G. L.; Sanchez, C. Nanocellulose, a Versatile Green Platform: From Biosources to Materials and Their Applications. *Chem. Rev.* **2018**, *118*, 11575-11625.
- (26) Chen, W.; Yu, H.; Lee, S.-Y.; Wei, T.; Li, J.; Fan, Z. Nanocellulose: a promising nanomaterial for advanced electrochemical energy storage. *Chem. Soc. Rev.* **2018**, *47*, 2837-2872.
- (27) Du, H. S.; Liu, W.; Zhang, M.; Si, C.; Zhang, X.; Li, B. Cellulose nanocrystals and cellulose nanofibrils based hydrogels for biomedical applications. *Carbohydr. Polym.* **2019**, *209*, 130-144.
- (28) Curvello, R.; Raghuwanshi, V. S.; Garnier, G. Engineering nanocellulose hydrogels for biomedical applications. *Adv. Colloid Interface Sci.* **2019**, *267*, 47-61.
- (29) Chen, Y.; Zhang, L.; Yang, Y.; Pang, B.; Xu, W.; Duan, G.; Jiang, S.; Zhang, K. Recent Progress on Nanocellulose Aerogels: Preparation, Modification, Composite Fabrication, Applications. *Adv. Mater.* **2021**, *33*, 2005569.
- (30) Yadav, C.; Saini, A.; Zhang, W.; You, X.; Chauhan, I.; Mohanty, P.; Li, X. Plant-based nanocellulose: A review of routine and recent preparation methods with current progress in its applications as rheology modifier and 3D bioprinting, *Int. J. Biol. Macromol.* **2021**, *166*, 1586-1616.

- (31) Ning, N. Y.; Wang, Z.; Yao, Y.; Zhang, L.; Tian, M. Enhanced electromechanical performance of bio-based gelatin/glycerin dielectric elastomer by cellulose nanocrystals. *Carbohydr. Polym.* **2015**, *130*, 262-267.
- (32) Rodrigues, A. P. H.; Pereira, I. M.; de Souza, S. D.; Brey Gil C. S.; Machado, G.; Carvalho, S. M.; Pereira, F. V.; Paiva, P. R. P.; de Oliveira, L. C. A.; de O. Patricio, P. S. Control of properties of nanocomposites bio-based collagen and cellulose nanocrystals. *Cellulose* **2017**, *24*, 1731-1744.
- (33) Rudisill, S. G.; DiVito, M. D.; Hubel, A.; Stein, A. In vitro collagen fibril alignment via incorporation of nanocrystalline cellulose. *Acta Biomater.* **2015**, *12*, 122-128.
- (34) Xiao, Y.; Liu, Y.; Wang, Y.; Jin, Y.; Guo, X.; Liu, Y.; Qi, X.; Lei, H.; Xu, H. Heat-induced whey protein isolate gels improved by cellulose nanocrystals: Gelling properties and microstructure. *Carbohydr. Polym.* **2020**, *231*, 115749.
- (35) Brown, E. E.; Hu, D.; Lail, N. A.; Zhang, X. Potential of Nanocrystalline Cellulose-Fibrin Nanocomposites for Artificial Vascular Graft Applications. *Biomacromolecules* **2013**, *14*, 1063-1071.
- (36) Kargarzadeh, H.; Mariano, M.; Huang, J.; Lin, N.; Ahmad, I.; Dufresne, A. Thomas, S. Recent developments on nanocellulose reinforced polymer nanocomposites: A review. *Polymer* **2017**, *132*, 368-393.
- (37) Miao, C.; Hamad, W. Y. Critical insights into the reinforcement potential of cellulose nanocrystals in polymer nanocomposites. *Curr. Opin. Solid State Mater. Sci.* **2019**, *23*, 100761
- (38) De France, K.; Zeng, Z.; Wu, T.; Nyström, G. Functional Materials from Nanocellulose: Utilizing Structure–Property Relationships in Bottom-Up Fabrication. *Adv. Mater.* **2020**, 2000657.

- (39) Lou, Y. R.; Kanninen, L.; Kuisma, T.; Niklander, J.; Noon, L. A.; Burks, D.; Urtti, A.; Yliperttula, M. The Use of Nanofibrillar Cellulose Hydrogel As a Flexible Three-Dimensional Model to Culture Human Pluripotent Stem Cells. *Stem Cells Dev.* **2014**, *23*, 380-392.
- (40) Hua, K.; Lindström, T.; Mihranyan, A.; Stromme, M.; Ferraz, N. Surface Chemistry of Nanocellulose Fibers Directs Monocyte/Macrophage Response. *Biomacromolecules.* **2015**, *16*, 2787-2795.
- (41) Nakayama, K. H.; Shayan, M.; Huang, N. F. Engineering Biomimetic Materials for Skeletal Muscle Repair and Regeneration. *Adv. Healthc. Mater.* **2019**, *8*, 1801168.
- (42) BM29 BIOSAXS.  
[http://www.esrf.eu/home/UsersAndScience/Experiments/MX/About\\_our\\_beamlines/bm29.html](http://www.esrf.eu/home/UsersAndScience/Experiments/MX/About_our_beamlines/bm29.html)  
(access date: 03/29/2021).
- (43) Pernot, P.; Round, A.; Barrett, R.; De Maria Antolinos, A.; Gobbo, A.; Gordon, E.; Huet, J.; Kieffer, J.; Lentini, M.; Mattenet, M.; Morawe, C.; Mueller-Dieckmann, C.; Ohlsson, S.; Schmid, W.; Surr, J.; Theveneau, P.; Zerrad L.; McSweeney, S. Upgraded ESRF BM29 beamline for SAXS on macromolecules in solution. *J. Synchrotron Radiat.* **2013**, *20*, 660-664.
- (44) Round, A.; Felisaz, F.; Fodinger, L.; Gobbo, A.; Huet, J.; Villard, C.; Blanchet, C. E.; Pernot, P.; McSweeney, S.; Roessle, M.; Svergun, D. I.; Cipriani, F. BioSAXS Sample Changer: a robotic sample changer for rapid and reliable high-throughput X-ray solution scattering experiments *Acta Crystallogr. Sect. D* **2015**, *71*, 67-75.
- (45) Ashiotis, G.; Deschildre, A.; Nawaz, Z.; Wright, J. P.; Karkoulis, D.; Picca, F. E.; Kieffer, J. The fast azimuthal integration Python library: pyFAI. *J. Appl. Crystallogr.* **2015**, *48*, 510-519.



- (46) Chen, Y.; Mao, H.; Zhang, X.; Gong, Y.; Zhao, N. Thermal conformational changes of bovine fibrinogen by differential scanning calorimetry and circular dichroism. *Int. J. Biol. Macromol.* **1999**, *26*, 129-134.
- (47) Wasilewska, M.; Adamczyk, Z.; Jachimska, B. Structure of Fibrinogen in Electrolyte Solutions Derived from Dynamic Light Scattering (DLS) and Viscosity Measurements *Langmuir*, **2009**, *25*, 3698–3704.
- (48) Phan-Xuan, T.; Thuresson, A.; Skepö, M.; Labrador, A.; Bordes, R.; Matic, A. Aggregation behavior of aqueous cellulose nanocrystals: the effect of inorganic salts. *Cellulose* **2016**, *23*, 3653-3663.
- (49) Boluk, Y.; Danumah, C. Analysis of cellulose nanocrystal rod length by dynamic light scattering and electron microscopy. *J. Nanopart. Res.* **2014**, *16*, 2174.
- (50) Uhlig, M.; Fall, A.; Wellert, S.; Lehmann, M.; Prévost, S.; Wagberg, L.; v. Klitzing, R.; Nyström, G. Two-Dimensional Aggregation and Semi-Dilute Ordering in Cellulose Nanocrystals. *Langmuir* **2016**, *32*, 442-450.
- (51) Ogzulu, H.; Danumah, C.; Boluk, Y. Colloidal behavior of aqueous cellulose nanocrystal suspensions. *Curr. Opin. Colloid Interface Sci.* **2017**, *29*, 46-56.
- (52) Gudapati, H.; Parisi, D.; Colby, R. H.; Ozlobat, I. T. Rheological investigation of collagen, fibrinogen and thrombin solutions for drop-on-demand 3D bioprinting. *Soft Matter* **2020**, *16*, 10506-10517.
- (53) Stamboroski, S.; Joshi, A.; Noeske, P.-L. M.; Köppen, S.; Brüggemann, D. Principles of Fibrinogen Fiber Assembly In Vitro. *Macromol. Biosci.* **2021**, 2000412.

- (54) Lombardo, S.; Thielemans, W. Thermodynamics of adsorption on nanocellulose surfaces. *Cellulose* **2019**, *26*, 249-279.
- (55) Lopez, M.; Bizot, H.; Chambat, G.; Marais, M.-F.; Zykwinska, A. ; Ralet, M.-C. ; Driguez, H. ; Buléon, A. Enthalpic Studies of Xyloglucan-Cellulose Interactions. *Biomacromolecules* **2010**, *11*, 1417-1428.
- (56) Sivaraman, B.; Fears, K. P.; Latour, R. A. Investigation of the Effects of Surface Chemistry and Solution Concentration on the Conformation of Adsorbed Proteins Using an Improved Circular Dichroism Method. *Langmuir* **2009**, *25*, 3050-3056.
- (57) Rysava, J.; Dyr, J. E ; Homola, J.; Dostalek, J. ; Krizova, P. ; Masova, L. ; Suttnar, J. ; Briestensky, J.; Santar, I.; Myska, K.; Pecka, M. Surface interactions of oxidized cellulose with fibrin(ogen) and blood platelets. *Sens. Actuator B* **2003**, *90*, 243-249.
- (58) Bettadapur, A.; Suh, G. C.; Geisse, N. A.; Wang, E. R.; Hua, C.; Huber, H. A.; Viscio, A. A.; Kim, J. Y.; Strickland, J. B.; McCain, M. L. Prolonged Culture of Aligned Skeletal Myotubes on Micromolded Gelatin Hydrogels. *Sci. Rep.* **2016**, *28*, 28855.
- (59) Duffy, R. M.; Sun, Y.; Feinberg, A. W. Understanding the Role of ECM Protein Composition and Geometric Micropatterning for Engineering Human Skeletal Muscle. *Ann. Biomed. Eng.* **2016**, *44*, 2076-2089.
- (60) Boontheekul, T.; Hill, E. E.; Kong, H.-J.; Mooney, D. J. Regulating Myoblast Phenotype Through Controlled Gel Stiffness and Degradation. *Tissue Eng.* **2007**, *13*, 1431-1442.

- (61) Ross, J. J.; Tranquillo, R. T. ECM gene expression correlates with in vitro tissue growth and development in fibrin gel remodeled by neonatal smooth muscle cells. *Matrix Biol.* **2003**, *22*, 477-490.
- (62) Wang, K.; Albert, K.; Mosser, G.; Haye, B.; Percot, A.; Paris, C.; Peccate, C.; Trichet, L.; Coradin, T. Self-assembly/condensation interplay in nano-to-microfibrillar silicified fibrin hydrogels. *Int. J. Biol. Macromol.* **2020**, *164*, 1422-1431.
- (63) Guex, A. G.; Kocher, F. M. ; Fortunato, G.; Körner, E.; Hegemann, D.; Carrel, T. P.; Tevaearai, H. T.; Giraud, M. N. Fine-tuning of substrate architecture and surface chemistry promotes muscle tissue development. *Acta Biomater.* **2012**, *8*, 1481-1489.
- (64) Dugan, J. M.; Gough, J. E.; Eichhorn, S. J. Directing the morphology and differentiation of skeletal muscle cells using oriented cellulose nanowhiskers. *Biomacromolecules* **2010**, *11*, 2498-2504.
- (65) Ryl, A.; Owczarz, P. Injectability of Themosensitive, Low-Concentrated Chitosan Colloids as Flow Phenomenon through the Capillary under High Shear Rate Conditions. *Polymers* **2020**, *12*, 2260.